

Fractionalization of Majorana-Ising-type quasiparticles

J.E. Sanches,^{1,*} L.T. Lustosa,¹ L.S. Ricco,² I.A. Shelykh,^{2,3} M. de Souza,⁴ M.S. Figueira,⁵ and A.C. Seridonio^{1,†}

¹*São Paulo State University (Unesp), School of Engineering,*

Department of Physics and Chemistry, 15385-000, Ilha Solteira-SP, Brazil

²*Science Institute, University of Iceland, Dunhagi-3, IS-107, Reykjavik, Iceland*

³*ITMO University, St. Petersburg, 197101, Russia*

⁴*São Paulo State University (Unesp), IGCE, Department of Physics, 13506-970, Rio Claro-SP, Brazil*

⁵*Instituto de Física, Universidade Federal Fluminense, 24210-340, Niterói, Rio de Janeiro, Brazil*

We theoretically investigate the spectral properties of a quantum impurity (QI) hosting the here proposed Majorana-Ising-type quasiparticle (MIQ). It arises from the coupling between a finite topological superconductor (TSC) based on a chain of magnetic adatoms-superconducting hybrid system and an integer large spin S flanking the QI. Noteworthy, the spin S couples to the QI via the Ising-type exchange interaction. As the TSC chain contains overlapped Majorana zero-modes (MZMs) at the edges, we counterintuitively find a regime wherein the Ising term modulates the isolation of a fractionalized and resonant MZM at the QI site. Interestingly enough, the fermionic nature of this state is revealed as purely of electron tunneling-type and most astonishingly, it completely ignores the Andreev reflection process in its birth. We find that an isolated edge state appears as a zero-mode in a finite TSC and hope that it could be used in *majorana*-based quantum computing.

I. INTRODUCTION

Majorana fermions are peculiar particles equal to their own antiparticles described by real solutions of the Dirac equation[1]. In Condensed Matter Physics, such fermions rise as quasiparticle excitations usually quoted as Majorana zero-modes (MZMs), which are found attached to the boundaries of topological superconductors (TSCs)[2–31]. Astonishingly, since the theoretical Kitaev seminal proposal of *p-wave* superconductivity[32], MZMs are notably coveted due to their attribution as building-blocks for the highly pursued fault-tolerant topological quantum computing. Thereafter, in the last years, such excitations have received astounding focus from both communities working with quantum science and technology.

Interestingly enough, theoretical predictions ensure that the fractional zero-bias peak (ZBP) given by the conductance $\mathcal{G}_{\text{Total}}(0) = \frac{e^2}{2h}$ in transport evaluations through quantum dots[2–4], if robust against perturbations, could be regarded as the capital hallmark of an isolated MZM at the edge of a TSC[3, 4]. Once an ordinary fermion can be decomposed into two MZMs, the amplitude $1/2$ in $\mathcal{G}_{\text{Total}}(0)$ fractionalizes the quantum of conductance $\frac{e^2}{h}$ and represents the electronic zero-frequency spectral weight, which reveals indeed, the MZM “half-fermionic” nature. This aforementioned fingerprint is expected to show up in engineered platforms that combine conventional *s-wave* superconductivity and spin-texture [see Refs.[33–35] and Fig.1(a)]. As aftermath, the *p-wave* superconductivity becomes feasible, thus allowing the experimental realization of the spinless Kitaev wire, which is indeed, a TSC in 1D[7, 25, 27, 32, 36–39]. For such an accomplishment, we highlight two practical recipes,

which have the following ingredients: (i) a semiconducting nanowire, with strong spin-orbit coupling (SOC) and under a magnetic field, should be deposited on top of an *s-wave* superconductor[25, 29–31, 36, 37, 40] or (ii) a linear chain of magnetic adatoms with exchange interactions should be hosted by an *s-wave* superconductor with strong SOC[13, 18, 33–35, 41–46]. In both the situations, the *s-wave* superconductors with singlet Cooper pairing lead to the so-called superconducting proximity effect, which is pivotal to carry forward the superconducting (SC) character into such manufactured Kitaev wires. Thus, the Zeeman field from the previous recipes (i) and (ii), together with the magnified SOC from such quantum materials, establish a synergy that stabilizes the system spin-texture. Consequently, the triplet Cooper pairing for the *p-wave* superconductivity, as well.

Particularly in the topological nontrivial regime of such setups, these Majorana quasiparticle excitations emerge ideally, i.e., as MZMs decoupled from each other and localized on the boundaries of the TSC. Due to this decoupling from their environment, MZMs are regarded robust against perturbations, once they are topologically protected by the SC gap. Thus, MZMs become promising candidates for a quantum computing free of the decoherence phenomenon[47, 48]. However, perfectly far apart MZMs are hypothetical objects, since they are reliable solely in infinite-size systems and in real experiments, the quantum wires are finite. As a result, these end MZMs within a finite length overlap with each other and inevitably, a fermionic mode with a finite energy emerges instead.

To overcome the aforementioned challenge, in this work, we find as route the fractionalization of ordinary MZMs, in particular, those found at a quantum impurity (QI) site coupled to one edge of a finite TSC in 1D. To this end, we should take into account the Ising exchange interaction between an integer large spin and such a QI. This setup corresponds to Figs.1(a) and (b),

* corresponding author: jose.sanches@unesp.br

† corresponding author: antonio.seridonio@unesp.br

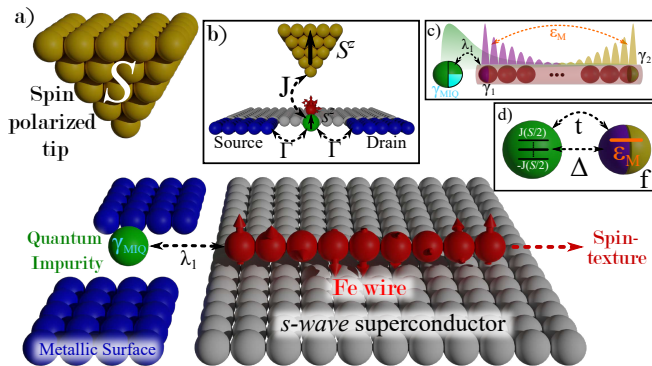


Figure 1. (a) Proposed device expected to show a Majorana-Ising-type quasiparticle (MIQ) γ_{MIQ} localized at the quantum impurity (QI) site. The MIQ leads to a zero-bias conductance peak $\mathcal{G}_{\text{MIQ}}(0) = \frac{e^2}{4h}$ due to the QI placed between source and drain leads, but the total conductance is still $\mathcal{G}_{\text{Total}}(0) = \frac{e^2}{2h}$. This occurs once a genuine electron tunneling process is present and there is a complete lack of local Andreev reflection. It can be performed by considering the QI simultaneously coupled to a spin-polarized tip with an integer large spin S via an Ising-type exchange interaction J and with a hopping term λ_1 to a helical spin-texture chain hosted by an s -wave superconductor. (b) Side view of panel (a) wherein the QI-lead coupling Γ and Ising-type exchange interaction J for the spin-polarized tip and QI appear highlighted. (c) Pictorial scheme of panel (b), which effectively consists of a topological superconductor (TSC), where ϵ_M represents the overlap between the Majorana zero-modes (MZMs) γ_1 and γ_2 at edges, while the QI shows the MIQ γ_{MIQ} . The spatial distributions of the wave functions for the MZMs and QI are also illustrated. The factor $\frac{1}{4}$ in \mathcal{G}_{MIQ} has correspondence to the $\frac{1}{4}$ from the volume for the sphere depicted to represent the quasiparticle γ_{MIQ} , in contrast to the ratio $\frac{1}{2}$ for the typical volume of the MZMs γ_1 and γ_2 . (d) These MZMs mimic a delocalized fermionic site f , wherein ϵ_M plays the role of its energy level, while the QI has $2S + 1$ levels ranging from $-J(S/2)$ to $+J(S/2)$. In this scenario, such quantum dots constitute a Kitaev dimer, i.e., with hopping t and pairing Δ of the p -wave Cooper pair split into the QI and f orbitals.

and it contains the ordinary MZMs γ_1 and γ_2 placed at the edges of a short TSC wire. To better understand our findings, we propose to view the MZMs as sketched in Fig.1(c), where these objects appear symbolized by calottes (half-spheres). We clarify that the employment of such a pictorial representation for the MZMs aims to explain diagrammatically the electron fractionalization into them, as well as the MZM fractionalization itself here observed. These calottes belong to a delocalized sphere cut in half, with each part placed at the TSC edges. This cartoon is very useful and it has the purpose of emulating the nonlocal nature of the fermionic state composed by these MZMs, which are found spatially far apart. To best of our knowledge, the Majorana zero-frequency spectral weight, in particular for a QI coupled to an infinite TSC, is given by the unity when the leaking of the MZM γ_1 into a quantum dot occurs[4]. This unity

corresponds to a calotte, which is a half-electron state that contributes to the conductance $\mathcal{G}_{\text{MZM}}(0) = \frac{e^2}{2h}$, as expected[3, 4]. Particularly for a finite TSC, we define as the system sweet spot [see Fig.3 b)-I] a special configuration, in which a peculiar Ising exchange interaction allows us to observe a fractionalized MZM quasiparticle γ_{MIQ} at the QI, namely, the called by us as Majorana-Ising-type quasiparticle (MIQ) [Figs.1(a) and (c)]. This quasiparticle can be viewed as the half-calotte within the cartoon representation of the QI state [see also Fig.1(c)]. Such a ratio symbolizes a novel MZM-type excitation in the presence of finite TSCs, in which technically speaking, it is identified by a Majorana zero-frequency spectral weight equals to half. Equivalently, the same amount corresponds to $\frac{1}{4}$ of the entire QI electronic state. In contrast, it leads to $\mathcal{G}_{\text{MIQ}}(0) = \frac{e^2}{4h}$ as it should be. Interestingly enough, solely in one of the Majorana densities of states (DOSs) of the QI, the MIQ becomes evident as a resonant mode localized at $\omega = 0$. Counterintuitively, the other Majorana DOS of the QI instead of exhibiting a resonant state, reveals a Majorana zero-frequency spectral weight with a valley, but presenting the same magnitude of the resonant Majorana fermion. In this manner, we can safely state that this novel MZM-type quasiparticle, i.e., the MIQ, is then found at the QI. In this situation, we demonstrate that the emergence of such a quasiparticle yields a zero-bias local Andreev conductance entirely null, with only normal electronic contribution to the total conductance.

II. THE MODEL

The effective system Hamiltonian that corresponds to the proposed setup presented in Fig.1(a) can be expressed as:

$$\begin{aligned} \mathcal{H} = & \sum_{\alpha k \sigma} \epsilon_{\alpha k} c_{\alpha k \sigma}^\dagger c_{\alpha k \sigma} + \sum_{\sigma} \epsilon_{\sigma} d_{\sigma}^\dagger d_{\sigma} + i \epsilon_M \gamma_1 \gamma_2 \\ & + \left(\frac{\Gamma}{2\pi\rho_0} \right)^{1/2} \sum_{\alpha k \sigma} (c_{\alpha k \sigma}^\dagger d_{\sigma} + \text{H.c.}) + J s^z S^z \\ & + \lambda_1 (d_{\uparrow} - d_{\downarrow}^\dagger) \gamma_1, \end{aligned} \quad (1)$$

where the operator $c_{\alpha k \sigma}^\dagger$ ($c_{\alpha k \sigma}$) describes the creation (annihilation) of an electron with momentum k , spin- z $\sigma = \pm 1$, energy $\epsilon_{\alpha k} = \epsilon_k - \mu_{\alpha}$ for the metallic lead $\alpha = [\text{Source}, \text{Drain}]$ in terms of the single-particle energy ϵ_k and chemical potential μ_{α} , while d_{σ}^\dagger (d_{σ}) stands for the electrons at the QI site in which ϵ_{σ} represents their energy levels per spin. To connect the QI to the metallic leads and a large spin S as well, we should consider the QI-lead coupling $\Gamma = 2\pi v^2 \rho_0$, which is determined by the QI-lead hopping term v and lead DOS ρ_0 , in parallel to the Ising-type exchange interaction J [Fig.1(b)]. This Ising Hamiltonian involves the components s^z and S^z of the QI ($s = 1/2$) and S , respectively, wherein the latter

could be well-represented, within an experimental framework, by a spin-polarized tip [Ref.[49] and Figs.1(a)-(b)]. The emergence of MZMs at the TSC wire edges are accounted for γ_1 and γ_2 , with ε_M as the overlap parameter. Finally, λ_1 couples the spin-up channel of the QI to γ_1 [Fig.1(c)]. Additionally, for the sake of simplicity, we consider that the spin-down degree is decoupled from the TSC and obeys the single impurity Anderson model (SIAM)[50]. Thus, we assume that the spin component of the QI that couples to the Kitaev wire is $\sigma = +1$, which is, as can be viewed in Fig.1(a), the same spin direction assumed for the edges of the magnetic chain of adatoms. This means that the spin-flips of the QI electron injected into the TSC and vice-versa are prevented. Therefore, the spin-up degree of the QI is the unique to perceive the TSC. Different spin-textures on the TSC edge where γ_1 is found[51], which would allow the mixing of the spin degrees of freedom, will be addressed elsewhere and do not belong to the current analysis. However, even with the present assumption, we shall see that both these spin components become influenced by S and that the TSC mimics an effective quantum dot tunnel and Andreev-coupled to the QI [Fig.1(d)].

To this end, we call the attention that the Majorana and Ising terms of Eq.(1) should be conveniently rewritten to access the system underlying Physics: (i) the Ising term turns straightforwardly into

$$J s^z S^z = \frac{J}{2} \sum_{m\sigma} \sigma m d_\sigma^\dagger d_\sigma |m\rangle \langle m|, \quad (2)$$

due to the standard expansions $s^z = \frac{1}{2} \sum_\sigma \sigma d_\sigma^\dagger d_\sigma$ and $S^z = \sum_m m |m\rangle \langle m|$ with $m = [-S, -S+1, \dots, S-1, S]$ for the QI and large spin, respectively. This means that each spin channel in the QI acquires a multi-level structure split into $2S+1$ energies ranging from $-J(S/2)$ to $+J(S/2)$. As a matter of fact, the TSC alters this feature quite a bit for the channel $\sigma = +1$ as we shall see in the numerical data; and (ii) it is imperative to evoke that the MZMs are made by the electron (f^\dagger) and hole (f) of a regular Dirac fermion delocalized over the TSC edges, which lead to $\gamma_1 = \frac{1}{\sqrt{2}}(f^\dagger + f)$ and $\gamma_2 = \frac{i}{\sqrt{2}}(f^\dagger - f)$. In this picture, ε_M plays the role of the energy level related to the electronic occupation $f^\dagger f$ and the QI is indeed hybridized with f , as mentioned earlier, via the hopping t and the superconducting pairing Δ . In summary, by considering the gauge $\lambda_1 = \sqrt{2}t$ and $\Delta = t$ [Fig.1(d)], we simply find the Kitaev dimer composed by d_\uparrow and f orbitals:

$$\begin{aligned} i\varepsilon_M \gamma_1 \gamma_2 + \varepsilon_\uparrow d_\uparrow^\dagger d_\uparrow + \lambda_1 (d_\uparrow - d_\uparrow^\dagger) \gamma_1 &= \varepsilon_M (f^\dagger f - \frac{1}{2}) \\ + \varepsilon_\uparrow d_\uparrow^\dagger d_\uparrow + (t d_\uparrow f^\dagger + \Delta d_\uparrow f + \text{H.c.}). \end{aligned} \quad (3)$$

Similarly, the spin-up channel of the QI can be also decomposed in MZMs[4], which we label by γ_A and γ_B , i.e.,

$$d_\uparrow = \frac{1}{\sqrt{2}}(\gamma_A + i\gamma_B). \quad (4)$$

Based on Eq.(4), one can compute the Majorana zero-frequency spectral weights for γ_A and γ_B , respectively. These quantities reveal that in the topological nontrivial regime ($J = 0$, $\Delta = t$ and $\varepsilon_M = \varepsilon_\uparrow = 0$)[4, 32] for the Kitaev dimer, that at the QI site, one spectral weight shows a unitary amplitude for a resonant zero-mode, while the other is completely null at zero-energy. It means that an isolated MZM is found at the QI. Analogously, such a feature is also observed in f [4, 32]. This results, according to Eq.(3) given by $i\sqrt{2}\lambda_1\gamma_B\gamma_1$, into two isolated MZMs spatially placed at d_\uparrow and f , namely, γ_A and γ_2 , respectively. For the trivial case ($\varepsilon_M \neq 0$), the two spectral weights for γ_A and γ_B attain to unity and then, two resonant zero-modes emerge at the QI site. Thus, Eq.(4) is extremely clarifying, once it points out the possibility of having within the QI, in the presence of ε_M and J , the isolation of the here proposed MIQ. Additionally, as one can notice, the spin down channel always shows the trivial case, due to its decoupling from the TSC. For completeness, the MZMs for d_\downarrow we label by γ_C and γ_D .

III. QUANTUM TRANSPORT AND GREEN'S FUNCTIONS

In this section, our goal is the analytical evaluation of the total conductance through the QI device depicted in Figs.1(a)-(b). As a matter of fact, solely the spin-up channel contributes to the conductance, once the spin-down is energetically inaccessible as previously stated. In the case of a grounded TSC, symmetric QI-lead couplings (Γ) independent of the bias-voltage eV and $\mu_{\text{Source}} = -\mu_{\text{Drain}} = eV/2$, the crossed Andreev reflection is suppressed and the conductance can be split into[52]

$$\mathcal{G}_{\text{Total}} = \mathcal{G}_{\text{ET}} + \mathcal{G}_{\text{LAR}}, \quad (5)$$

where ET and LAR stand for the electron tunneling and local Andreev reflection processes, respectively, with

$$\mathcal{G}_{\text{ET}}(eV) = \frac{e^2}{2h} [\tau_{\alpha\bar{\alpha}}^{\text{ET}}(eV/2) + \tau_{\alpha\bar{\alpha}}^{\text{ET}}(-eV/2)], \quad (6)$$

wherein $\alpha = \text{Source}$, $\bar{\alpha} = \text{Drain}$ and vice-versa, together with

$$\mathcal{G}_{\text{LAR}}(eV) = \frac{e^2}{2h} [\tau_{\alpha\alpha}^{\text{LAR}}(eV/2) + \tau_{\alpha\alpha}^{\text{LAR}}(-eV/2)], \quad (7)$$

in which the transmittances $\tau_{\alpha\bar{\alpha}}^{\text{ET}} = (2S+1)\Gamma^2 |\langle\langle d_\uparrow | d_\uparrow^\dagger \rangle\rangle|^2$ and $\tau_{\alpha\alpha}^{\text{LAR}} = (2S+1)\Gamma^2 |\langle\langle d_\uparrow^\dagger | d_\uparrow^\dagger \rangle\rangle|^2$ depend on the Green's functions (GFs) of type $\langle\langle A_\sigma | B_\sigma \rangle\rangle = \sum_m \langle\langle A_\sigma | m \rangle\rangle \langle\langle m | B_\sigma \rangle\rangle$ (details in the Appendix), due to the presence of the large spin, in which the thermal average $\langle\langle |m\rangle \langle m| \rangle\rangle = \frac{1}{2S+1}$ should be taken into account. They should be determined via of the standard equation-of-motion (EOM) approach[53] summarized as

$$\omega^+ \langle\langle A_\sigma | B_\sigma \rangle\rangle = \langle\langle [A_\sigma, B_\sigma]_+ \rangle\rangle + \langle\langle [A_\sigma, \mathcal{H}] | B_\sigma \rangle\rangle, \quad (8)$$

where $\omega^+ = \omega + i\eta^+$ and $\eta^+ \rightarrow 0$. Additionally, Ref.[52] also ensures that the QI normalized DOS obeys the decomposition

$$\text{DOS}(\uparrow) = -\Gamma \text{Im} \langle \langle d_\uparrow | d_\uparrow^\dagger \rangle \rangle = \tau_{\alpha\bar{\alpha}}^{\text{ET}} + \tau_{\alpha\bar{\alpha}}^{\text{LAR}}. \quad (9)$$

As Eq.(9) is bounded to unity, it describes the electronic overall transmittance through the QI decomposed into ET and LAR processes. Specially when it attains to its maximum value at zero energy, i.e., the $\text{DOS}(\uparrow)(0) = 1$ value gives the electronic zero-frequency spectral weight. In this case, the regular fermionic state of the QI is then made equally by the MZMs γ_A and γ_B . Equivalently, it means that the corresponding normalized DOSs for such quasiparticles localize Majorana states with the same spectral weights and as a result, the QI state is fully built by a pair of resonant MZMs. It gives rise to the conductance $\mathcal{G}_{\text{Total}}(0) = \frac{e^2}{h}$. Interestingly enough for $\text{DOS}(\uparrow)(0) = 1/2$, an isolated ordinary MZM is found at the QI site and the zero-bias conductance is characterized by the hallmark $\mathcal{G}_{\text{Total}}(0) = \frac{e^2}{2h}$ [3, 4]. Such a case corresponds to an ideal infinite superconducting wire. However, as we shall see, there is a regime in which the value $\text{DOS}(\uparrow)(0) = 1/2$ is still present for a finite wire and due to the Ising interaction between the large spin and the QI, the observation of the conductance $\mathcal{G}_{\text{Total}}(0) = \frac{e^2}{2h}$ is ensured. This emerges from the novel excitation that we introduce as the MIQ, in particular, by driving the system into the sweet spot for the exchange interaction J , namely, $J = J_h$. In the latter, the index ‘‘h’’ stands for the ‘‘half-fermion’’ special condition of a MZM, which is produced by imposing $\text{DOS}(\uparrow)(0) = 1/2$, from where we extract J_h for a given S [see Fig.3 b)-I].

Therefore, in order to reveal the aforementioned Physics about the system conductance, we should begin evaluating Eq.(6) for the electron tunneling process. Thus, the GF $\langle \langle d_\uparrow | d_\uparrow^\dagger \rangle \rangle$ should be found via the EOM method, which gives

$$\langle \langle d_\uparrow | d_\uparrow^\dagger \rangle \rangle = \frac{1}{2S+1} \sum_m \frac{1}{\omega^+ - \varepsilon_\uparrow - \frac{Jm}{2} + i\Gamma - \Sigma_{\text{MFs}}^{+m}}, \quad (10)$$

where $\Sigma_{\text{MFs}}^{+m} = K_+ + (2t\Delta)^2 K_{\text{MFs}} \tilde{K}_m$ represents the self-energy correction due to the couplings of the QI with the TSC and the large spin S . This also depends on the following defined quantities

$$K_{\text{MFs}} = \frac{\omega^+}{\omega^2 - \varepsilon_M^2 + 2i\omega\eta^+ - (\eta^+)^2}, \quad (11)$$

$$K_\pm = \frac{\omega^+ (\Delta^2 + t^2) \pm \varepsilon_M (t^2 - \Delta^2)}{\omega^2 - \varepsilon_M^2 + 2i\omega\eta^+ - (\eta^+)^2} \quad (12)$$

and

$$\tilde{K}_m = \frac{K_{\text{MFs}}}{\omega^+ + \varepsilon_\uparrow + \frac{Jm}{2} + i\Gamma - K_-}. \quad (13)$$

Concerning the LAR, the conductance of Eq.(7) needs the evaluation of the anomalous GF $\langle \langle d_\uparrow^\dagger | d_\uparrow^\dagger \rangle \rangle$ instead. After performing the EOM approach, it gives rise to

$$\langle \langle d_\uparrow^\dagger | d_\uparrow^\dagger \rangle \rangle = -\frac{1}{2S+1} \sum_m \frac{2t\Delta K_m}{\omega^+ + \varepsilon_\uparrow + \frac{Jm}{2} + i\Gamma - \Sigma_{\text{MFs}}^{-m}}, \quad (14)$$

with $\Sigma_{\text{MFs}}^{-m} = K_- + (2t\Delta)^2 K_{\text{MFs}} K_m$ and

$$K_m = \frac{K_{\text{MFs}}}{\omega^+ - \varepsilon_\uparrow - \frac{Jm}{2} + i\Gamma - K_+}. \quad (15)$$

However, if we want to know about the possibility of isolating MZMs in the QI, the DOSs for γ_A and γ_B should be found in order to examine the emergence of resonant states. To this end, we invert Eq.(4) for γ_A and γ_B , namely, $\gamma_A = (d_\uparrow^\dagger + d_\uparrow)/\sqrt{2}$ and $\gamma_B = i(d_\uparrow^\dagger - d_\uparrow)/\sqrt{2}$, and later on we calculate the GFs $\langle \langle \gamma_A | \gamma_A \rangle \rangle$ and $\langle \langle \gamma_B | \gamma_B \rangle \rangle$. Consequently,

$$\begin{aligned} \langle \langle \gamma_j | \gamma_j \rangle \rangle &= \frac{1}{2} [\langle \langle d_\uparrow | d_\uparrow^\dagger \rangle \rangle + \langle \langle d_\uparrow^\dagger | d_\uparrow \rangle \rangle \\ &\quad + \epsilon (\langle \langle d_\uparrow^\dagger | d_\uparrow^\dagger \rangle \rangle + \langle \langle d_\uparrow | d_\uparrow \rangle \rangle)], \end{aligned} \quad (16)$$

where $j = (A, B)$ corresponds to $\epsilon = (+1, -1)$, respectively. Physically speaking, the sign reversal in ϵ can lead to distinct quantum interference phenomena, in particular between those encoded by the normal GFs ($\langle \langle d_\uparrow | d_\uparrow^\dagger \rangle \rangle$ and $\langle \langle d_\uparrow^\dagger | d_\uparrow \rangle \rangle$) and the corresponding superconducting ($\langle \langle d_\uparrow^\dagger | d_\uparrow^\dagger \rangle \rangle$ and $\langle \langle d_\uparrow | d_\uparrow \rangle \rangle$). To reveal such interference processes, we need just to find the GFs $\langle \langle d_\uparrow^\dagger | d_\uparrow \rangle \rangle$ and $\langle \langle d_\uparrow | d_\uparrow \rangle \rangle$ to close the evaluation of $\langle \langle \gamma_A | \gamma_A \rangle \rangle$ and $\langle \langle \gamma_B | \gamma_B \rangle \rangle$. By applying the EOM method, we conclude that

$$\langle \langle d_\uparrow^\dagger | d_\uparrow \rangle \rangle = \frac{1}{2S+1} \sum_m \frac{1}{\omega^+ + \varepsilon_\uparrow + \frac{Jm}{2} + i\Gamma - \Sigma_{\text{MFs}}^{-m}} \quad (17)$$

and

$$\langle \langle d_\uparrow | d_\uparrow \rangle \rangle = -\frac{1}{2S+1} \sum_m \frac{2\Delta t \tilde{K}_m}{\omega^+ - \varepsilon_\uparrow - \frac{Jm}{2} + i\Gamma - \Sigma_{\text{MFs}}^{+m}}. \quad (18)$$

Naturally, we define the normalized DOSs for γ_A and γ_B such as

$$\text{DOS}(\uparrow)[\gamma_j] = -\Gamma \text{Im} \langle \langle \gamma_j | \gamma_j \rangle \rangle. \quad (19)$$

This formula elucidates that when the quantity $\text{DOS}(\uparrow)[\gamma_j](0) = -\Gamma \text{Im} \langle \langle \gamma_j | \gamma_j \rangle \rangle(0) = 1$ is fulfilled, it can be recognized as the maximum Majorana quasiparticle transmittance or its corresponding zero-frequency spectral weight.

Henceforward, we focus the attention on the case $\varepsilon_\uparrow = 0$ (grounded SC). We perceive by inspecting Eqs.(10) and

(17), that Eq.(9) becomes also $\text{DOS}(\uparrow) = -\Gamma\text{Im}\langle\langle d_{\uparrow}^{\dagger}|d_{\uparrow}\rangle\rangle$. Additionally, $-\Gamma\text{Im}\langle\langle d_{\uparrow}^{\dagger}|d_{\uparrow}^{\dagger}\rangle\rangle = -\Gamma\text{Im}\langle\langle d_{\uparrow}|d_{\uparrow}\rangle\rangle$. This in combination with Eqs.(16) and (19) allow us to establish that

$$\text{DOS}(\uparrow) = \frac{1}{2}(\text{DOS}(\uparrow)[\gamma_A] + \text{DOS}(\uparrow)[\gamma_B]). \quad (20)$$

Consequently, by taking into account this finding together with Eqs.(5), (6), (7) and (9), we conclude the providential equality as follows

$$\mathcal{G}_{\text{Total}} = \mathcal{G}_{\gamma_A} + \mathcal{G}_{\gamma_B}, \quad (21)$$

where

$$\mathcal{G}_{\gamma_j}(\text{eV}) = \frac{e^2}{4h}[\text{DOS}(\uparrow)[\gamma_j](\text{eV}/2) + \text{DOS}(\uparrow)[\gamma_j](\text{-eV}/2)] \quad (22)$$

stands for the conductance contribution arising from the quasiparticle γ_j within the QI.

We highlight that Eq.(21) introduces an alternative perspective concerning the underlying Physics of the conductance in Eq.(5): the ET and LAR quantum transport mechanisms are revealed as the net effect of two Majorana quasiparticle conductances, namely, the corresponding contributions arising from γ_A and γ_B , respectively. In this context, we shall see that our main findings hold for the constraint $J = J_h$ fulfilled, thus characterizing the system sweet spot to produce the MIQ. This regime consists of the maximum Majorana quasiparticle transmittance $\text{DOS}(\uparrow)[\gamma_j](0) = 1$, surprisingly, fractionalized and split into $\text{DOS}(\uparrow)[\gamma_A](0) = 1/2$ and $\text{DOS}(\uparrow)[\gamma_B](0) = 1/2$. Despite such equipartition, the electronic transmittance is still given by $\text{DOS}(\uparrow)(0) = 1/2$ [see Fig.3 b)-I] and according to Eq.(22), it ensures $\mathcal{G}_{\gamma_A}(0) = \frac{e^2}{4h}$ and $\mathcal{G}_{\gamma_B}(0) = \frac{e^2}{4h}$. However, counterintuitively, as we shall see, solely $\mathcal{G}_{\gamma_B}(0)$ contains a MZM in the common sense, i.e., a resonant state, while $\mathcal{G}_{\gamma_A}(0)$ shows a dip instead, but with the same magnitude of the peak in γ_B . This is the reason why we call the contribution $\mathcal{G}_{\gamma_B}(0) = \frac{e^2}{4h}$ by $\mathcal{G}_{\text{MIQ}}(0)$, in attention to the emergent MIQ. This is the unique MZM-type resonant state that appears in the system, due to the interplay between the topological superconductivity and the Ising Hamiltonian. In this case, Eqs.(5) and (21) ensure that when the MIQ emerges, $\mathcal{G}_{\gamma_B}(0)$ exhibits a maximum and $\mathcal{G}_{\gamma_A}(0)$ shows a minimum, in such a way that only $\mathcal{G}_{\text{ET}}(0)$ enters into $\mathcal{G}_{\text{Total}}(0) = \frac{e^2}{2h}$. It means that the LAR process is found entirely suppressed within this regime. The complete analysis here summarized will be discussed in detail later on.

IV. RESULTS

In the entire numerical analysis we keep constant $\varepsilon_{\uparrow} = 0$ (grounded SC), $\lambda_1 = 2.12\Gamma$ and perform variations in

the parameters ε_M , S and J . In Fig.2 we present, for the QI of Fig.1, the total conductance of Eq.(5) as a function of the bias-voltage eV/Γ . Particularly in Fig.2(a) the ideal case is considered, i.e., the TSC wire is perfectly infinite ($\varepsilon_M = 0$) and the large spin is found turned-off ($S = 0$). This case is well-known, being characterized by the ZBP in the conductance given by $\mathcal{G}_{\text{Total}}(0) = \frac{e^2}{2h}$ [3, 4]. Interestingly enough, this ZBP in the conductance represents the isolated MZM γ_1 originally attached to one edge of the TSC wire, which leaks towards the QI site in the form of the MZM γ_A . The MZM leakage from the TSC edge into the QI is then characterized by the $\text{DOS}(\uparrow)[\gamma_A](0) = 1$ and $\text{DOS}(\uparrow)[\gamma_B](0) = 0$. We will provide, later on, extra details concerning this issue in the discussion of the inset a)-I of Fig.3(a). In the other hand, the satellite peaks in Fig.2(a) are the aftermath of the splitting arising from the condition $i\sqrt{2}\lambda_1\gamma_B\gamma_1$ given by Eq.(3) for the topological nontrivial regime of the system. Additionally, we have made explicit via Eq.(5) that the ET and LAR processes compose the total conductance. Thus, such a feature can be viewed in Fig.2(b), where we notice, in particular, for the ZBP conductance that, the ET and LAR split equally. Here we propose that it is still achievable to obtain $\mathcal{G}_{\text{Total}}(0) = \frac{e^2}{2h}$ for a finite TSC wire and to perform also the isolation of a Majorana quasiparticle at the QI site. In our setup, such an excitation rises, in particular, dressed by the Ising interaction. To this end, an integer large spin S should be accounted for and be coupled to the QI with a special value in the exchange interaction J . Thus, by evaluating $J = J_h$, the amplitude $\mathcal{G}_{\text{Total}}(0) = \frac{e^2}{2h}$ [Eq.(21)] finally becomes restored. However, we will verify that such a configuration corresponds to isolate a peculiar MZM, namely γ_B , with a resonant peak characterized by the spectral weight $\text{DOS}(\uparrow)[\gamma_B](0) = 1/2$ [Eq.(19)], while for γ_A we have the same amplitude, i.e., $\text{DOS}(\uparrow)[\gamma_A](0) = 1/2$, but with a dip instead.

Now, we consider the presence of a large spin S . Figs.2(c) and (d) show the total conductance in the presence of $S = 3$ and $J_h = 1.335\Gamma$ [see inset b)-I of Fig.3(b)] for a finite TSC with $\varepsilon_M = \Gamma$. The ZBP conductance in Fig.2(c) is $\mathcal{G}_{\text{Total}}(0) = \frac{e^2}{2h}$ as expected, but the decomposition into ET and LAR channels described in Fig.2(d) reveals a striking result: solely ET survives, while LAR is completely suppressed at zero-bias. Below we will verify that the LAR suppression corresponds to a quasiparticle localization in the DOS for γ_B , which leads to $\text{DOS}(\uparrow)[\gamma_B](0) = 1/2$. Thus, according to Eq.(22), such a finite DOS contributes to a conductance $\mathcal{G}_{\gamma_B}(0) = \mathcal{G}_{\text{MIQ}}(0) = \frac{e^2}{4h}$, where we define the MIQ $\gamma_B \equiv \gamma_{\text{MIQ}}$.

In order to understand the emergence of the MIQ, we begin with the trivial case in Fig.3(a): the central panel discriminates the electronic $\text{DOS}(\uparrow)$ into the corresponding DOSs for γ_A and γ_B [Eq.(19)] with $S = 0$ and $\varepsilon_M = \Gamma$. This case is regarded as trivial, once we verify that in both the DOSs γ_A and γ_B resonant states pinned

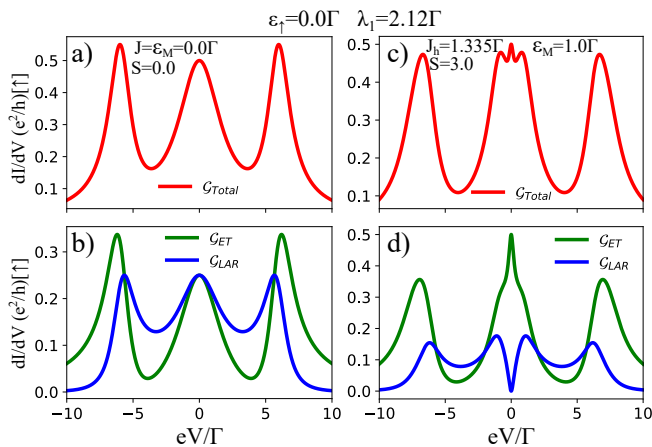


Figure 2. (Color online) (a) Total differential conductance $\mathcal{G}_{\text{Total}}$ [Eq.(5)] versus the source-drain bias-voltage eV in units of the QI-lead coupling Γ with isolated MZMs γ_1 and γ_2 ($\varepsilon_M = 0$) in the absence of a spin-polarized tip ($S = 0$). As aftermath, a zero-bias peak (ZBP) emerges with amplitude $\mathcal{G}_{\text{Total}}(0) = \frac{e^2}{2h}$ and characterizes the leaking of the MZM γ_1 from the TSC wire edge [Fig.1(c)] into the QI as γ_A [inset a)-I of Fig.3(a) and Refs.[3, 4]]. (b) The ZBP conductance can be split into finite contributions from the electron tunneling (ET) and local Andreev reflection (LAR) processes [Eq.(5)], namely, $\mathcal{G}_{\text{ET}}(0)$ and $\mathcal{G}_{\text{LAR}}(0)$, respectively. This corresponds to the ideal case of an infinite TSC wire, wherein these processes compete on equal footing. (c) In the presence of a tip with $S = 3$ and exchange coupling at the sweet spot $J = J_h = 1.335\Gamma$ [inset b)-I of Fig.3(b)] for a finite wire ($\varepsilon_M = 1\Gamma$), the amplitude $\mathcal{G}_{\text{Total}}(0) = \frac{e^2}{2h}$ is still observed and denotes the existence of a MIQ γ_{MIQ} within the QI, but with related differential conductance $\mathcal{G}_{\text{MIQ}}(0) = \frac{e^2}{4h}$ [Fig.3(c) and Eqs.(21)-(22)]. (d) In the regime of (c), $\mathcal{G}_{\text{LAR}}(0)$ is completely quenched and solely the term $\mathcal{G}_{\text{ET}}(0)$ contributes to the ZBP.

at zero-energy $\omega = 0$ are present. Schematically, the QI fermionic state can be imagined as a sphere formed by two MZMs depicted by two calottes. This is the manner we outline pictorially the two zero-energy resonant states, the so-called MZMs in the DOSs γ_A and γ_B . This sketch can be found in the upper-right inset of Fig.3(a), in which each calotte symbolizes the “half-fermionic” character of the MZM. Equivalently, a calotte occupies the half-volume of the sphere and as it corresponds to a MZM, it can be surely characterized by $\text{DOS}(\uparrow)[\gamma_j](0) = 1$. As aftermath, according to Eqs.(20)-(22), these two MZMs lead to the zero-bias conductance peak $\mathcal{G}_{\text{Total}}(0) = \frac{e^2}{h}$. Concerning the satellite peaks in the $\text{DOS}(\uparrow)[\gamma_B]$, they occur due to the overlap between the MZMs γ_B and γ_1 . In the other hand, the inset panel a)-II of Fig.3(a) shows the spin-down channel, which is the one decoupled from the TSC. To analyze it on the same footing as the spin-up channel, we assume $\varepsilon_\downarrow = 0$ and verifies that both the MZMs γ_C and γ_D , which constitute this spin sector of the QI, are then identified exactly by degenerate resonant states. The evaluation of the DOSs for the spin-down sector just employs the GFs for the spin-

up sector, but it disregards the superconducting terms. As none of these MZMs overlap with γ_1 , a full superposition of the lineshapes for these MZMs manifests in the profiles of the DOSs γ_C and γ_D . Therefore, satellite peaks do not emerge. Now, let us go back to discuss the spin-up channel. We should pay particular attention to the case $\varepsilon_M = 0$ depicted in the inset panel a)-I of Fig.3(a), which corresponds to the nonoverlapped situation between γ_1 and γ_2 . This scenario is the ideal one and it contains the pillars for the conductance behavior of Fig.2(a). Notice that γ_B overlaps with γ_1 leading to satellite peaks in $\text{DOS}(\uparrow)[\gamma_B]$ and $\text{DOS}(\uparrow)[\gamma_B](0) = 0$, while γ_A is found isolated and localized as a well-defined resonant zero-mode with spectral weight $\text{DOS}(\uparrow)[\gamma_A](0) = 1$. Thereafter, $\mathcal{G}_{\text{Total}}(0) = \mathcal{G}_{\gamma_A}(0) = \frac{e^2}{2h}$. This case is well-known in literature [3, 4] and points out that the MZM γ_A contributes to the conductance as a resonant state in contrast to γ_B , which shows a gap in $\text{DOS}(\uparrow)[\gamma_B]$ around zero-bias. This latter prevents a finite conductance, i.e., $\mathcal{G}_{\gamma_B}(0) = 0$. Below, we will see that by turning-on the exchange J for a given S , the spectral profiles for the $\text{DOS}(\uparrow)[\gamma_A]$ and $\text{DOS}(\uparrow)[\gamma_B]$ will exhibit a multi-level structure. Additionally, these densities will be responsible, according to Eq.(22), by a nonquantized $\mathcal{G}_{\text{Total}}(0) \neq \frac{e^2}{h}$ in Eq.(21). In the situation of arbitrary J , the contributions to $\mathcal{G}_{\text{Total}}(0) \neq 0$ will not arise from well-defined resonant zero-mode states in $\text{DOS}(\uparrow)[\gamma_A]$ and $\text{DOS}(\uparrow)[\gamma_B]$. As we shall see next, the Majorana fermion localization within the QI as a resonant zero-mode state will only occur for the sweet spot $J = J_h$.

Fig.3(b) treats the presence of a large spin coupled to the QI for $\varepsilon_M = \Gamma$. As we can notice, the Ising interaction $J = 5\Gamma$ for $S = 3$ clearly affects the spectral profiles of $\text{DOS}(\uparrow)[\gamma_A]$ and $\text{DOS}(\uparrow)[\gamma_B]$. Basically, it introduces a multi-level structure for the satellite peaks and modifies drastically the MZM localization around the zero-bias. Surprisingly, the $\text{DOS}(\uparrow)[\gamma_A]$ presents a valley (dip) at zero-energy and a quasi-resonant MZM rises in $\text{DOS}(\uparrow)[\gamma_B]$. As a matter of fact, the latter cannot be considered a well-defined resonant MZM: its spectral weight is not exactly an integer or semi-integer number, and the lineshape broadening does not obey a *lorentzian-like* form to define a quasiparticle lifetime[38]. The lineshapes of such spectral densities are then distinct, but counterintuitively, their zero-bias values coincide, i.e., $\text{DOS}(\uparrow)[\gamma_A](0) = \text{DOS}(\uparrow)[\gamma_B](0)$. As the spin-up sector of the QI is the one coupled to the TSC, the spectral profiles in the $\text{DOS}(\uparrow)[\gamma_A]$ and $\text{DOS}(\uparrow)[\gamma_B]$ do not follow strictly the standard angular momentum theory for the Zeeman splitting [Eq.(2)]. Usually, this theory ensures that for an integer S , $2S$ symmetrically displaced levels around the corresponding at $\omega = \varepsilon_\uparrow = 0$ should emerge. Here, indeed we observe a mirror-symmetric set with S energy bands below and above the zero-bias, respectively, where nearby peculiar spectral structures rise. We reveal that the profiles differ significantly in this range, as aftermath of the nontrivial interplay between the TSC and Ising exchange term. In Figs.4(d)-

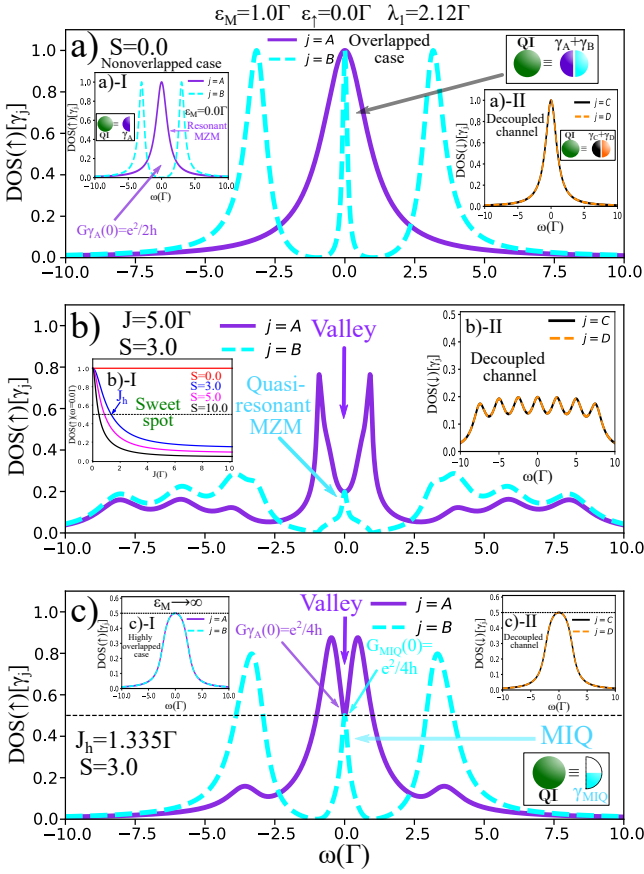


Figure 3. (Color online) (a) The central panel shows the frequency dependence of the normalized densities of states (DOSs) for the MZMs γ_A and γ_B [Eq.(19)] for the spin-up channel within the QI by assuming the spin-polarized tip absent and the MZMs γ_1 and γ_2 overlapped ($\varepsilon_M = 1\Gamma$) in the TSC. In each DOS we find a resonant MZM, which corresponds to a “half-fermionic” state of the QI depicted as the green sphere in the upper-right inset. This sphere has inner MZMs represented by calottes to denote the half-fermion nature of the MZM. In the nonoverlapped situation, only the calotte γ_A prevails [inset a)-I]. It leads to $\mathcal{G}_{\text{Total}}(0) = \mathcal{G}_{\gamma_A}(0) = \frac{e^2}{2h}$ in Fig.2(a) [Eqs.(21)-(22)]. For the spin-down channel, which is decoupled from the TSC, the MZMs γ_C and γ_D within the QI stay paired permanently [inset a)-II]. (b) In the presence of $S = 3$ and $J = 5\Gamma$ for $\varepsilon_M = 1\Gamma$ the DOS for γ_A changes drastically exhibiting a valley at $\omega = 0$ instead of a peak, while for γ_B the zero-mode is not-well defined. To restore the ZBP $\mathcal{G}_{\text{Total}}(0) = \frac{e^2}{2h}$ we should choose the right J for a given S , i.e., the sweet spot $J = J_h$ [panel b)-I] for the QI DOS of Eq.(20) imposing $\text{DOS}(\uparrow)(0) = 1/2$. In the spin-down channel, the γ_C and γ_D DOSs are degenerate with a $2S + 1$ multi-level structure [panel b)-II]. (c) The choice $J = J_h = 1.335\Gamma$ for $S = 3$ completely defines the valley and peak for the DOSs γ_A and γ_B , respectively, where in the latter we introduce $\gamma_B \equiv \gamma_{\text{MIQ}}$ as the Majorana-Ising quasiparticle, once the peak clearly represents the unique MZM isolated in the system. It is characterized by a ZBP given by $\mathcal{G}_{\text{MIQ}}(0) = \frac{e^2}{4h}$ pictorially illustrated by the half-calotte in the lower-right inset for the green sphere representing the QI fermionic state. However, $\mathcal{G}_{\text{Total}}(0) = \mathcal{G}_{\gamma_A}(0) + \mathcal{G}_{\text{MIQ}}(0) = \frac{e^2}{2h}$.

(f) we will see that the manifestation of this effect relies within a region comprised by *cone-like walls* spanned by ω and ε_M in the DOSs of the system. Within the cone, the Zeeman splitting becomes unusual and the energy spacing between the levels is simultaneously governed by J and ε_M . Besides, solely the spin-down channel shows standard Zeeman splitting, once it does not perceive the TSC. This can be verified in the inset panel b)-II of Fig.3(b), where the DOSs for γ_C and γ_D , as expected, present the ordinary $2S + 1$ multi-level structure ensured by Eq.(2). We highlight that upon decreasing the exchange parameter J , the restoration of the conductance $\mathcal{G}_{\text{Total}}(0) = \frac{e^2}{2h}$ can be still allowed. Thus, we should remember that such a conductance arises from the fulfillment of the condition $\text{DOS}(\uparrow)(0) = 1/2$. Particularly in the inset panel b)-I of Fig.3(b), we show exactly the points where this happens by considering several values of S and $\varepsilon_M \neq 0$. Particularly for $S = 3$, this sweet spot occurs for $J = J_h = 1.335\Gamma$ and its dependence on ε_M is revealed as very weak according to our numerical calculations (not shown). It means that $J = J_h = 1.335\Gamma$ still keeps the value $\text{DOS}(\uparrow)(0) = 1/2$ while ε_M does not exceed very much Γ ($\varepsilon_M \gg \Gamma$). Experimentally speaking, J can be tuned by changing the tip-QI vertical distance. Thus for $\varepsilon_M \neq 0$, $\mathcal{G}_{\text{Total}}(0)$ drops from $\frac{e^2}{h}$ to $\frac{e^2}{2h}$ when $J = J_h$. Hence, at the sweet spot, if one knows previously the spin S of the tip, J_h can be extracted from Fig.3 b)-I or vice-versa.

In Fig.3(c) we present the case $J = J_h = 1.335\Gamma$ that leads to our main finding: a perfect localization of a resonant state at zero-energy in $\text{DOS}(\uparrow)[\gamma_B]$, with spectral weight $\text{DOS}(\uparrow)[\gamma_B](0) = 1/2$. The latter amplitude points out that the ordinary MZM now is fractionalized and the value $\text{DOS}(\uparrow)[\gamma_B](0) = 1$ is not present anymore. This fractionalized MZM, the called MIQ by us, then leads to a conductance $\mathcal{G}_{\gamma_B}(0) = \mathcal{G}_{\text{MIQ}}(0) = \frac{e^2}{4h}$ as ensured by Eq.(22). The value $\text{DOS}(\uparrow)[\gamma_B](0) = 1/2$ can be pictorially viewed by the half-calotte found in the lower-right inset of Fig.3(c), which symbolizes the MZM fractionalization within the QI state. Nevertheless, to complete the total conductance $\mathcal{G}_{\text{Total}}(0) = \frac{e^2}{2h}$, the zero-bias value for $\text{DOS}(\uparrow)[\gamma_A](0)$ should coincide, i.e., $\text{DOS}(\uparrow)[\gamma_A](0) = 1/2$ and as aftermath, $\mathcal{G}_{\gamma_A}(0) = \frac{e^2}{4h}$ as well. Here we emphasize that in $\text{DOS}(\uparrow)[\gamma_A](0)$ a quantum destructive interference manifests and a resonant state does not rise at zero-bias. Moreover, it is capital to clarify the underlying mechanism to produce the MIQ: the key idea is the decrease of J , thus forcing the merge of the $2S$ side bands (satellite peaks) of the system towards the zero-energy, where a resonant level is pinned. As a result, this sum of amplitudes for the satellite peaks interferes constructively at zero-energy giving rise to $\text{DOS}(\uparrow)(0) = 1/2$ for $J = J_h$. Further, our findings do not depend on the sign of J and in case of a semi-integer large spin, the multi-level structure is odd and a zero-energy is absent in the spectrum. In this manner, the MIQ cannot be excited. Concerning the inset pan-

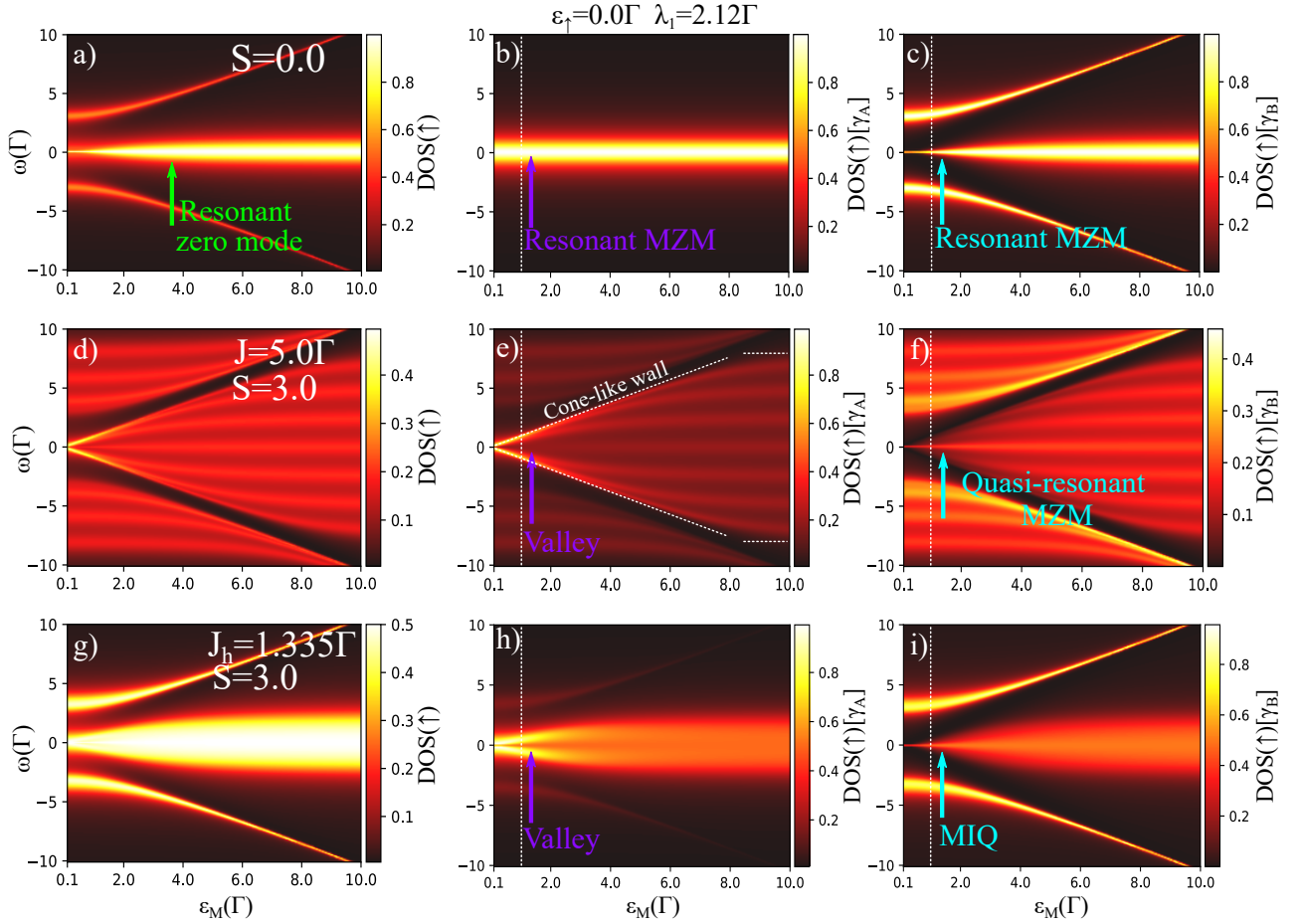


Figure 4. (Color online) Color maps of Eqs.(9) and (19) for the QI, γ_A and γ_B DOSs, respectively, spanned by the frequency ω and ε_M : (a) In the case $S = 0$, the ZBP in the DOS(\uparrow) arises from the individual ZBPs found in DOS(\uparrow)[γ_A] [panel(b)] and DOS(\uparrow)[γ_B] [panel(c)], due to the MZMs γ_A and γ_B that act as the building-blocks of the QI state $\varepsilon_\uparrow = 0$ [Eq.(20)]. They reveal that the system does not contain isolated MZMs and that the overlapped γ_1 and γ_2 split the zero-mode energy state leading to the upper and lower arcs in panels (a) and (c). Panels (d)-(f) reveal the influence of $S = 3$ and $J = 5\Gamma$ on the QI, where we can clearly see a $2S + 1$ multi-level structure centered at $\omega = 0$. The upper and lower arcs, distinctly, show $2S$ levels each. The central region of (e) has a valley-type structure in contrast to that for (f), which points out a quasi-resonant MZM. In both the cases, the $2S + 1$ multi-level structure is delimited by cone-like walls up to a threshold in ε_M (not indicated), where above it the DOS(\uparrow)[γ_A] and DOS(\uparrow)[γ_B] exhibit a zero-mode with the lines of the walls parallel to each other. For this situation, the TSC plays no role and the MZMs γ_A and γ_B stay paired as in (a)-(c). Panels (g)-(i) hold for the sweet spot $J = J_h = 1.335\Gamma$, where we have the zero-frequency valley and peak well-resolved in the DOS(\uparrow)[γ_A] and DOS(\uparrow)[γ_B], respectively. In the latter, the MIQ rises as aftermath of the partial merge of the $2S + 1$ multi-level structure centered at $\omega = 0$ upon decreasing the coupling J . We call the attention that the vertical lines represent slice cuts of the cases profoundly explored in Figs.2 and 3.

els c)-I and c)-II of Fig.3(c), we verify that for $\varepsilon_M \gg \Gamma$ (or $\varepsilon_M \rightarrow \infty$) the DOSs for the Majorana fermions are degenerate. For extremely short TSC wires ($\varepsilon_M \rightarrow \infty$), the energy level ε_M for the orbital f [Eq.(3)] is highly off resonance the QI energy $\varepsilon_\uparrow = 0$, thus making the QI and the TSC to decouple from each other. Thus, the spin-up channel behaves as the corresponding spin-down, which is the one permanently decoupled from the TSC. This implies that the MIQ cannot be seen for very short wires.

Fig.4 summarizes our findings exhibiting color maps of Eqs.(9) and (19) for the electronic and Majorana DOSs, respectively and spanned by ω and ε_M . Panels (a)-(c) de-

scribe the case $S = 0$, which is characterized by $\text{DOS}(\uparrow)(0) = 1$ and $\text{DOS}(\uparrow)[\gamma_A](0) = \text{DOS}(\uparrow)[\gamma_B](0) = 1$. This corresponds to the trivial regime where two MZMs localize around zero-bias and appear at the QI site. Such a characteristic relies in the zero-bias peaks and appears as horizontal lines in the representation of panels (a)-(c) for any finite value of ε_M . As we can see, the satellite peaks in (a) arise from (c). By turning-on the Ising interaction with $S = 3$ and $J = 5\Gamma$, the spectral profiles of the DOSs acquire distinct patterns: the satellite peaks obey approximately the standard angular momentum theory for the Zeeman splitting, thus exhibiting $2S$ split side-bands. In this situation, the linear dependence on the exchange

parameter J is lacking. Besides, the central regions of panels (a)-(c) are converted into the domains delimited by *cone-like walls* as those found in (d)-(f). While these walls persist up to a threshold in ε_M (not marked in the figure), a sophisticated interplay between the TSC and the Ising interaction rules the Physics of the system and allows the possibility of the MIQ existence. Notice that for $\varepsilon_M > \Gamma$, a $2S + 1$ multi-level central structure finally becomes resolved. It is worth mentioning that for $\varepsilon_M = \Gamma$, the line cuts in Fig.4 given by the vertical dashed lines, then correspond to the cases discussed in detail in Fig.3. In panels (e) and (f) we notice the rising of the valley and the quasi-resonant MZM spectral structures, respectively upon increasing ε_M . However, much above the threshold in ε_M , the linear spacing in J for the Zeeman splitting is restored and this situation is that delimited by the marked horizontal dashed lines. Finally, panels (g)-(i) show the merge of the multi-level structure in the sweet spot $J = J_h = 1.335\Gamma$ leading to the emergence of the MIQ in the Majorana channel γ_B , while the valley continues in the channel γ_A . Therefore, within *the cone-like walls* domain, the sector γ_B of Majorana fermions for the QI makes explicit a constructive interference process at zero-bias, while the corresponding in γ_A displays a destructive behavior. In this regime, the conductance $\mathcal{G}_{\text{LAR}}(0)$ becomes fully quenched and just $\mathcal{G}_{\text{ET}}(0)$ contributes to $\mathcal{G}_{\text{Total}}(0) = \frac{e^2}{2h}$ [Fig.2(d)].

V. CONCLUSIONS

We found that the fractionalization of regular MZMs becomes a feasible task once an integer large spin S is exchange coupled to a quantum impurity, in particular when it acts as the new edge of a finite TSC in 1D. A counterintuitive regime arises due to a sweet value for the Ising coupling, which is capable of isolating a fractionalized MZM. We introduce such an excitation as the called Majorana-Ising-type quasiparticle (MIQ). As aftermath, we report the emergence of one MZM with the maximum spectral weight reduced by half and exhibiting resonant character. In contrast, the other MZM mode in the QI does not localize around zero-energy, but shows the same spectral weight of the resonant MZM via an antiresonant profile. Interestingly enough, due to the localization of the MIQ, half of the quantum conductance is made essentially by the normal electronic contribution, while that from the Andreev reflection is totally lacking in such a situation. This behavior differs from that observed in perfectly infinite TSC wires, in which one MZM localizes at QI site with maximum spectral weight given by unit and with electronic and Andreev conductances equally split at zero-bias. Therefore, our proposal points out a manner to induce, within a more realistic perspective from an experimental point of view, a quantum state at the edge of a short TSC in 1D. In this way, we expect that our MIQ can be employed as a potential building-block in *majorana*-based quantum computing.

VI. ACKNOWLEDGMENTS

We thank the Brazilian funding agencies CNPq (Grants. Nr. 302887/2020-2, 308410/2018-1, 311980/2021-0, 305668/2018-8 and 308695/2021-6), Coordenação de Aperfeiçoamento de Pessoal de Nível Superior - Brasil (CAPES) – Finance Code 001 and FAPERJ process Nr. 210 355/2018. LSR and IAS acknowledge the support from Icelandic Research Fund (Rannis), projects No. 163082-051 and “Hybrid polaritonics”. IAS also acknowledges support from the Program Priority 2030. LSR thanks ACS and Unesp for their hospitality.

Appendix A: Green’s functions

As the GFs in the presence of the large spin obey the notation $\langle\langle A_\sigma | B_\sigma \rangle\rangle = \sum_m \langle\langle A_\sigma | m \rangle\rangle \langle m | B_\sigma \rangle$ [54], here we make explicit the details in the EOM approach to find the elements of type $\langle\langle A_\sigma | m \rangle\rangle \langle m | B_\sigma \rangle$. In what follows, we have

$$\begin{aligned} & (\omega^+ - \varepsilon_\uparrow - \frac{Jm}{2} + i\Gamma) \langle\langle d_\uparrow | m \rangle\rangle \langle m | d_\uparrow^\dagger \rangle \\ &= \frac{1}{2S+1} - t \langle\langle f | m \rangle\rangle \langle m | d_\uparrow^\dagger \rangle - \Delta \langle\langle f^\dagger | m \rangle\rangle \langle m | d_\uparrow^\dagger \rangle, \end{aligned} \quad (\text{A1})$$

$$\begin{aligned} & (\omega^+ + \varepsilon_\uparrow + \frac{Jm}{2} + i\Gamma) \langle\langle d_\uparrow^\dagger | m \rangle\rangle \langle m | d_\uparrow \rangle \\ &= \frac{1}{2S+1} + t \langle\langle f^\dagger | m \rangle\rangle \langle m | d_\uparrow \rangle + \Delta \langle\langle f | m \rangle\rangle \langle m | d_\uparrow \rangle, \end{aligned} \quad (\text{A2})$$

the other two terms are given by

$$\begin{aligned} & (\omega^+ + \varepsilon_\uparrow + \frac{Jm}{2} + i\Gamma) \langle\langle d_\uparrow^\dagger | m \rangle\rangle \langle m | d_\uparrow^\dagger \rangle \\ &= t \langle\langle f^\dagger | m \rangle\rangle \langle m | d_\uparrow^\dagger \rangle + \Delta \langle\langle f | m \rangle\rangle \langle m | d_\uparrow^\dagger \rangle \end{aligned} \quad (\text{A3})$$

and

$$\begin{aligned} & (\omega^+ - \varepsilon_\uparrow - \frac{Jm}{2} + i\Gamma) \langle\langle d_\uparrow | m \rangle\rangle \langle m | d_\uparrow \rangle \\ &= -t \langle\langle f | m \rangle\rangle \langle m | d_\uparrow \rangle - \Delta \langle\langle f^\dagger | m \rangle\rangle \langle m | d_\uparrow \rangle \end{aligned} \quad (\text{A4})$$

And finally the last two GFs associated with the f site is

$$\begin{aligned} \langle\langle f | m \rangle\rangle \langle m | d_\uparrow \rangle &= \frac{-t}{(\omega^+ - \varepsilon_M)} \langle\langle d_\uparrow | m \rangle\rangle \langle m | d_\uparrow \rangle \\ &+ \frac{\Delta}{(\omega^+ - \varepsilon_M)} \langle\langle d_\uparrow^\dagger | m \rangle\rangle \langle m | d_\uparrow \rangle \end{aligned} \quad (\text{A5})$$

and

$$\begin{aligned} \langle\langle f^\dagger | m \rangle\rangle \langle m | d_\uparrow \rangle &= \frac{t}{(\omega^+ + \varepsilon_M)} \langle\langle d_\uparrow^\dagger | m \rangle\rangle \langle m | d_\uparrow \rangle \\ &- \frac{\Delta}{(\omega^+ + \varepsilon_M)} \langle\langle d_\uparrow | m \rangle\rangle \langle m | d_\uparrow \rangle. \end{aligned} \quad (\text{A6})$$

With this group of GFs we can determine the complete description of the QI.

-
- [1] E. Majorana, *Il Nuovo Cimento* (1924-1942) **14**, 10.1007/BF02961314 (1937).
- [2] P. Marra, *Journal of Applied Physics* **132**, 231101 (2022).
- [3] D. E. Liu and H. U. Baranger, *Phys. Rev. B* **84**, 201308 (2011).
- [4] E. Vernek, P. H. Penteado, A. C. Seridonio, and J. C. Egues, *Phys. Rev. B* **89**, 165314 (2014).
- [5] M. Duckheim and P. W. Brouwer, *Phys. Rev. B* **83**, 054513 (2011).
- [6] R. M. Lutchyn, J. D. Sau, and S. Das Sarma, *Phys. Rev. Lett.* **105**, 077001 (2010).
- [7] O. Lesser and Y. Oreg, *Journal of Physics D: Applied Physics* **55**, 164001 (2022).
- [8] F. Pientka, L. I. Glazman, and F. von Oppen, *Phys. Rev. B* **89**, 180505 (2014).
- [9] Y. Oreg, G. Refael, and F. von Oppen, *Phys. Rev. Lett.* **105**, 177002 (2010).
- [10] F. Pientka, L. I. Glazman, and F. von Oppen, *Phys. Rev. B* **88**, 155420 (2013).
- [11] J. Li, H. Chen, I. K. Drozdov, A. Yazdani, B. A. Bernevig, and A. H. MacDonald, *Phys. Rev. B* **90**, 235433 (2014).
- [12] J. Klinovaja, P. Stano, A. Yazdani, and D. Loss, *Phys. Rev. Lett.* **111**, 186805 (2013).
- [13] S. Nadj-Perge, I. K. Drozdov, B. A. Bernevig, and A. Yazdani, *Phys. Rev. B* **88**, 020407 (2013).
- [14] L. Fu and C. L. Kane, *Phys. Rev. B* **79**, 161408 (2009).
- [15] L. Fu and C. L. Kane, *Phys. Rev. Lett.* **100**, 096407 (2008).
- [16] M. M. Vazifeh and M. Franz, *Phys. Rev. Lett.* **111**, 206802 (2013).
- [17] S. Nakosai, Y. Tanaka, and N. Nagaosa, *Phys. Rev. B* **88**, 180503 (2013).
- [18] B. Braunecker and P. Simon, *Phys. Rev. Lett.* **111**, 147202 (2013).
- [19] A. C. Potter and P. A. Lee, *Phys. Rev. B* **85**, 094516 (2012).
- [20] S. B. Chung, H.-J. Zhang, X.-L. Qi, and S.-C. Zhang, *Phys. Rev. B* **84**, 060510 (2011).
- [21] C. W. J. Beenakker, *Rev. Mod. Phys.* **87**, 1037 (2015).
- [22] M. Sato and S. Fujimoto, *Journal of the Physical Society of Japan* **85**, 072001 (2016).
- [23] M. Sato and Y. Ando, *Reports on Progress in Physics* **80**, 076501 (2017).
- [24] A. Haim and Y. Oreg, *Physics Reports* **825**, 1 (2019), time-reversal-invariant topological superconductivity in one and two dimensions.
- [25] J. Alicea, *Reports on Progress in Physics* **75**, 076501 (2012).
- [26] C. Beenakker, *Annual Review of Condensed Matter Physics* **4**, 113 (2013).
- [27] A. S. Karsten Flensberg, Felix von Oppen, *Nature Reviews Materials* **6**, 944 (2021).
- [28] K. Laubscher and J. Klinovaja, *Journal of Applied Physics* **130**, 081101 (2021).
- [29] M. T. Deng, S. Vaitiekenas, E. B. Hansen, J. Danon, M. Leijnse, K. Flensberg, J. Nygard, P. Krogstrup, and C. M. Marcus, *Science* **354**, 1557 (2016).
- [30] V. Mourik, K. Zuo, S. M. Frolov, S. R. Plissard, E. P. A. M. Bakkers, and L. P. Kouwenhoven, *Science* **336**, 1003 (2012).
- [31] F. Nichele, A. C. C. Drachmann, A. M. Whiticar, E. C. T. O'Farrell, H. J. Suominen, A. Fornieri, T. Wang, G. C. Gardner, C. Thomas, A. T. Hatke, P. Krogstrup, M. J. Manfra, K. Flensberg, and C. M. Marcus, *Phys. Rev. Lett.* **119**, 136803 (2017).
- [32] A. Y. Kitaev, *Physics-Uspekhi* **44**, 131 (2001).
- [33] S. Nadj-Perge, I. K. Drozdov, J. Li, H. Chen, S. Jeon, J. Seo, A. H. MacDonald, B. A. Bernevig, and A. Yazdani, *Science* **346**, 602 (2014).
- [34] M. Ruby, F. Pientka, Y. Peng, F. von Oppen, B. W. Heinrich, and K. J. Franke, *Phys. Rev. Lett.* **115**, 197204 (2015).
- [35] R. Pawlak, M. Kisiel, J. Klinovaja, T. Meier, S. Kawai, T. Glatzel, D. Loss, and E. Meyer, *npj Quantum Information* **2**, 10.1038/npjqi.2016.35 (2016).
- [36] S. R. Elliott and M. Franz, *Rev. Mod. Phys.* **87**, 137 (2015).
- [37] R. Aguado, *LA RIVISTA DEL NUOVO CIMENTO* **40**, 523 (2017).
- [38] M. Leijnse and K. Flensberg, *Semiconductor Science and Technology* **27**, 124003 (2012).
- [39] T. D. Stanescu and S. Tewari, *Journal of Physics: Condensed Matter* **25**, 233201 (2013).
- [40] R. M. Lutchyn, J. D. Sau, and S. Das Sarma, *Phys. Rev. Lett.* **105**, 077001 (2010).
- [41] T.-P. Choy, J. M. Edge, A. R. Akhmerov, and C. W. J. Beenakker, *Phys. Rev. B* **84**, 195442 (2011).
- [42] J. Klinovaja, P. Stano, A. Yazdani, and D. Loss, *Phys. Rev. Lett.* **111**, 186805 (2013).
- [43] S. Jeon, Y. Xie, J. Li, Z. Wang, B. A. Bernevig, and A. Yazdani, *Science* **358**, 772 (2017).
- [44] P. Marra and M. Nitta, *Phys. Rev. B* **100**, 220502 (2019).
- [45] R. Pawlak, S. Hoffman, J. Klinovaja, D. Loss, and E. Meyer, *Progress in Particle and Nuclear Physics* **107**, 1 (2019).
- [46] B. Jäck, Y. Xie, and A. Yazdani, *Nature Reviews Physics* **3**, 2522 (2021).
- [47] C. Nayak, S. H. Simon, A. Stern, M. Freedman, and S. Das Sarma, *Rev. Mod. Phys.* **80**, 1083 (2008).
- [48] S. D. Sarma, M. Freedman, and C. Nayak, *npj Quantum Information* **1**, 2056 (2015).
- [49] R. Wiesendanger, *Rev. Mod. Phys.* **81**, 1495 (2009).
- [50] P. W. Anderson, *Phys. Rev.* **124**, 41 (1961).
- [51] E. Prada, R. Aguado, and P. San-Jose, *Phys. Rev. B* **96**, 085418 (2017).
- [52] L. Máthé, D. Sticlet, and L. P. Zárbo, *Phys. Rev. B* **105**, 155409 (2022).
- [53] H. Bruus and K. Flensberg, (Oxford: Oxford University Press) (2012).
- [54] D. N. Zubarev, *Soviet Physics Uspekhi* **3**, 320 (1960).